The Astrophysical Journal Supplement Series, 182:1–11, 2009 May doi:10.1088/0067-0049/182/1/1

AN EXPERIMENTAL INVESTIGATION OF THE DECOMPOSITION OF CARBON MONOXIDE AND FORMATION ROUTES TO CARBON DIOXIDE IN INTERSTELLAR ICES

Chris J. Bennett, Corey S. Jamieson, and Ralf I. Kaiser
Department of Chemistry, University of Hawaii at Manoa, Honolulu, HI 96822, USA; ralfk@hawaii.edu
Received 2008 October 3; accepted 2009 March 5; published 2009 April 15

ABSTRACT

The formation of carbon dioxide from the processing of carbon monoxide (CO) and molecular oxygen ($^{18}O_2$) via radiolysis is studied within the context of its formation in interstellar ices in quiescent clouds. With the help of isotopic labeling, we were able to "trace" the atoms and provide mechanistical information on how carbon monoxide is decomposed, and carbon dioxide is formed in interstellar ices. Here, we quantify the production of $^{18}O_3$, $O^{18}O_2$, $^{18}OO^{18}O$, $C^{18}O$, CO_2, ^{18}OCO, and $C^{18}O_2$. In contrast to experiments using ultraviolet irradiation, we find that upon exposure to energetic electrons, isolated carbon monoxide molecules are able to undergo unimolecular decomposition to give suprathermal carbon (C) and oxygen (O) atoms. Molecular oxygen decomposes to two oxygen atoms. The free oxygen atoms can react with carbon monoxide via addition to form the carbon dioxide isotopomers as observed experimentally. This mechanism to form carbon dioxide is distinctly different to the one observed in pure carbon monoxide ices where electronically excited carbon monoxide reacts with a neighboring carbon monoxide molecule to form solely carbon dioxide and a carbon atom.

Key words: astrochemistry – comets: general – cosmic rays – infrared: ISM – ISM: molecules – methods: laboratory – molecular processes

1. INTRODUCTION

The main focus of this paper is to provide insights into the formation and destruction mechanisms of carbon monoxide (CO) and carbon dioxide (CO_2) within interstellar ices. Both molecular compounds have long been recognized as constituents of molecular clouds in the gas phase (Wilson et al. 1970; d'Hendecourt & Jourdain de Muizon 1989) as well as components of the icy mantles of interstellar grains (Soifer et al. 1979; de Graauw et al. 1996). In the gas phase, carbon monoxide is the most abundant interstellar molecule besides molecular hydrogen, where the abundance ratio is typically of the order of 10^{-4}. Sheffer et al. (2008) recently produced sophisticated chemical models of a large number of both high- and low-density molecular clouds, whereby they were able to reproduce the column density of carbon monoxide in which they indicated that the two major reactions responsible for actually producing carbon monoxide were

$$CO^+ + H \rightarrow CO + H^+ \quad (1)$$

$$HCO^+ + e^- \rightarrow CO + H. \quad (2)$$

The depletion of gas-phase carbon monoxide is commonly associated with its adsorption onto interstellar grains during the collapse of a prestellar core (Aikawa et al. 2001, 2008). The abundance of carbon monoxide within interstellar ices from a recent survey of 23 infrared sources using the *Infrared Space Observatory* (*ISO*) showed its percentage composition typically between 3% and 25% relative to water (Gibb et al. 2004). Based on the fundamental band position and profile, the carbon monoxide molecule was found to reside in two different chemical environments: polar ices dominated by water and nonpolar ices where carbon monoxide is dominant, but other nonpolar species such as molecular nitrogen and molecular oxygen are thought to be also present but are infrared inactive. In the same survey, Gibb et al. also monitored solid carbon dioxide with typical abundances of 8%–35% relative to water, which was also found to be present within polar and nonpolar ices. Considering the fact that carbon dioxide is typically more abundant within interstellar ices than carbon monoxide, it is surprising that its gas-phase abundance is much lower, where the ratio of CO_2/H_2 is typically only a few 10^{-7} (Boonman et al. 2003). Even as a young stellar object begins to warm, triggering sublimation of the surrounding ices and releasing the volatile components to the gas phase the abundance of gas phase carbon dioxide is still very low (Dartois et al. 2000). This leads us to conclude that there must be very efficient destruction mechanisms (Talbi & Herbst 2002) such as a speculated reaction with hydrogen atoms to produce carbon monoxide and the hydroxyl radical:

$$CO_2 + H \rightarrow CO + OH. \quad (3)$$

Additionally, the formation of carbon dioxide in the gas phase is thought to be slow (Millar et al. 1991). This leads to the conclusion that it may only be efficiently formed either on the surface of icy grains or within the interstellar ices, most likely from precursors such as carbon monoxide, as well as the probable involvement of other oxygen bearing precursors such as water or molecular oxygen. Indeed, Pontoppidan (2006) reported that there is a direct correlation between the freeze-out of carbon monoxide onto interstellar grains and the increase in the abundance of carbon dioxide ices for several young stellar objects within the Oph-F star forming core.

Under the premise that carbon dioxide is formed from carbon monoxide within interstellar ices, we need to investigate how this process can actually occur. Let us first consider a reaction that could take place on the surface of a grain. Firstly, there is the possibility of an oxygen atom directly colliding with a surface-bound carbon monoxide molecule (the *Eley–Rideal* mechanism). Alternatively it is possible for the two species to condense onto the grain separately, and then migrate across the surface through diffusion until reaction occurs (the *Langmuir–Hinshelwood* mechanism). For processes such as

these, it is of paramount importance that they must occur without barrier, or with only a small barrier as some of the quiescent clouds where carbon dioxide ices have been found in high abundance have low temperatures of around 20 K (Whittet et al. 2007). Both these processes only occur on the *surface* of grains.

Fournier et al. (1979) utilized UV photons ($\lambda = 147$ nm; $E = 8.4$ eV) to irradiate a 1:1 mixture of dinitrogen monoxide (N_2O) with carbon monoxide dispersed within an argon matrix held at 7 K. Mass spectrometry was used to confirm the production of carbon dioxide at $m/z = 44$ (CO_2^+). They speculated that this could either be produced from reaction of carbon monoxide with electronically excited O(^{1}S) atoms or with ground-state O(^{3}P) atoms. The latter would help explain a thermoluminescence continuum (3800–5000 Å) which the sample began emitting when warmed to just 9 K. They proposed that through inter system crossing, the matrix may assist the following spin-forbidden process occurring via an excited triplet carbon dioxide species (not shown):

$$CO(X^1\Sigma^+) + O(^3P) \rightarrow CO_2\left(X^1\Sigma_g^+\right). \quad (4)$$

Thus, it was initially presumed in reaction models of grain-surface chemistry that the reaction had no entrance barrier (Tielens & Hagen 1982). However, subsequent experiments by Grim & d'Hendecourt (1986) gave contradictory results to this study. They subjected 1:1 mixture of CO:O_2 diluted in an argon matrix with UV photolysis ($\lambda = 115$–220 nm, $E = 5.6$–10.8 eV) at 10 K, which was then subsequently warmed to 28 K. They found that both carbon dioxide and ozone were produced during the irradiation period, but only ozone could be synthesized via diffusion of oxygen atoms during the warm-up process indicating that a barrier is indeed present for reaction (4), but showing that production via radiolysis may be a viable alternative formation mechanism. Later, Roser et al. (2001) were able to codeposit ^{18}O atoms (generated from radio-frequency dissociation of $^{18}O_2$) with ^{13}CO onto a surface at 5 K. Utilizing temperature programmed desorption and mass spectrometry, they monitored the channel at $m/z = 47$ ($^{18}O^{13}C^{16}O$). The experiment was repeated with the addition of a water-cap (~100 layers), delaying the sublimation temperature to ~150 K as compared to ~40 K for pure carbon monoxide. Here, the formation of carbon dioxide ($^{18}O^{13}C^{16}O$) was observed. They modeled the diffusion processes of both CO and O through a water lattice, whereby recombination could occur if they occupied the same cavity and overcame any energy barrier (if present). Their results indicated that the reaction barrier was around 290 K (0.02 eV). However, when Ruffle & Herbst (2001) attempted to model the formation of CO_2 ice around Elias 16, and reported that in order to fit the observed column density (Nummelin et al. 2001), the barrier for reaction (4) could not exceed 130 K (0.01 eV).

Because of the ambiguity considering the existence of a barrier for reaction (4), the potential energy surface of CO_2 has been subjected to several theoretical studies, most recently by Talbi et al. (2006) who carried out both high level ab initio and density functional calculations. For the gas-phase reaction, they reported the value for the barrier to be 49 kJ mol^{-1} (2970 K; 0.26 eV), an order of magnitude larger than that reported by Roser et al. (2001). They also considered the effects that surrounding water molecules may have on lowering the energy barrier, but reported that the effects were negligible, as previously reported (Woon 2002). It was also reported that the reaction between O(^{1}D) and CO($X^1\Sigma^+$) could form $CO_2(X^1\Sigma_g^+)$ without barrier, in agreement with previous studies (Xantheas & Ruedenberg 1994; Hwang & Mebel 2000).

Thus, the most attractive alternative is the formation of CO_2 from radiolysis via nonequilibrium chemistry. Indeed, there have been a large number of experiments studying the effects of UV radiation (Gerakines et al. 1996; Gerakines & Moore 2001; Cottin et al. 2003; Loeffler et al. 2005), MeV/keV ions (Baird 1972; Haring et al. 1984; Chrisey et al. 1986; Gerakines & Moore 2001; Trottier & Brooks 2004; Loeffler et al. 2005), and keV electrons (Jamieson et al. 2006a) on pure carbon monoxide ices. In addition to the formation of carbon dioxide, a variety of other species have been determined to be produced. Species identified by infrared spectroscopy include linear carbon chains such as C_3 and C_6, linear carbon oxide chains of the series C_nO ($n = 2-7$) as well as of the series C_nO_2 ($n = 3-5,7$), and ozone, O_3. It is interesting to note however, that the underlying mechanisms may vary between UV irradiation and ion/electron irradiation since only UV irradiation processes have to follow optical selection rules. As Gerakines & Moore (2001) suggested, MeV/keV ions (as well as keV electrons) are capable of dissociating the carbon monoxide molecule as depicted in reaction (5):

$$CO(X^1\Sigma^+) \rightarrow C(^3P/^1D) + O(^3P/^1D). \quad (5)$$

A recent experimentally determined value for this dissociation energy is given as 11.09 eV (Bakker & Parker 2000), and requires photons of wavelength below 112 nm for photodissociation to occur (Okabe 1978). A typical broadband hydrogen discharge lamp has the most intense band at 121 nm (10.2 eV; Lyman-α); this source has only considerable flux for photons within the range 7.3–10.5 eV (Muñoz Caro & Schutte 2003). It is obvious that a different mechanism is responsible for initiating the reactions. It has been considered that the most likely explanation is a two-step process, whereby a first photon excites the carbon monoxide into an excited state, which can then react with a neighboring carbon monoxide molecule to produce carbon dioxide and ground-state carbon atoms:

$$CO(X^1\Sigma^+) \rightarrow CO^* \quad (6)$$

$$CO^* + CO(X^1\Sigma^+) \rightarrow CO_2\left(X^1\Sigma_g^+\right) + C(^3P). \quad (7)$$

The reaction is endoergic by 5.64 eV, and there is experimental evidence supporting the fact that the excited state involved is the metastable $a^3\Pi$ state (Martin et al. 2000), which lies 6.0 eV above the ground state (Zetner et al. 1998). This production mechanism seems to support the species observed in experiments on the irradiation of carbon monoxide by UV photons (Gerakines et al. 1996; Gerakines & Moore 2001), in particular when carbon dioxide failed to be produced when exposed to irradiation within a nitrogen matrix (Cottin et al. 2003). It was also identified as a mechanistic pathway by Jamieson et al. (2006a) as the only destruction pathway when carbon monoxide ices were subjected to 5 keV electrons. This is supported by the fact that electron impact and inelastic energy loss processed by energetic electrons have been shown to excite carbon monoxide into the $a^3\Pi$ state (Zetner et al. 1998). But is there any evidence for reaction (5) proceeding within electron irradiated carbon monoxide ices?

In the present set of experiments, we aim to investigate the destruction processes of carbon monoxide, and also to address the question of whether free oxygen atoms can react with carbon monoxide to form carbon dioxide. We irradiated ice samples composed of carbon monoxide as well as isotopically enriched molecular oxygen ($^{18}O_2$) with 5 keV electrons. Refer to the discussion for a justification of using keV electrons as an irradiation source. From studying the kinetic profiles of the products produced we should be able to determine the destruction pathways of carbon monoxide and the formation mechanism of carbon dioxide.

2. EXPERIMENTAL DETAILS

The details of our experimental setup as well as the calculation of column densities and ice thicknesses can be found elsewhere (Bennett et al. 2004; Jamieson et al. 2006a). Briefly, the experiments are conducted in an ultrahigh vacuum (UHV) chamber where oil-free magnetically suspended pumps are used to bring the base pressure down to around 5×10^{-11} Torr. The gases are condensed onto a freely rotatable highly polished silver monocrystal situated in the center of the chamber which is cooled to 10 K by a closed cycle helium refrigerator. This condensed phase is sampled by a Nicolet 510 DX Fourier transform infrared (FTIR) spectrometer operating in absorption–reflection–absorption mode at a reflection angle of 75° (spectra are recorded in succession over the range 6000–400 cm^{-1} at a resolution of 2 cm^{-1}, each integrated over 2.5 min). Meanwhile, gaseous species may be analyzed by a quadrupole mass spectrometer (Balzer QMG 420) operating in residual gas analyzer mode.

In this case, the gas mixture under study consists of 136 mbar of carbon monoxide and 35 mbar of molecular oxygen ($^{18}O_2$). During the 3 min of condensation, these gases are deposited through a glass capillary array held 5 mm from the target, while the pressure in the main chamber was monitored at 1×10^{-7} Torr in order to give reproducible conditions. To calculate the resulting oxygen thickness, we approximated that the same condensation conditions hold as for a previous experiment where molecular oxygen was used (Bennett & Kaiser 2005). Here, pure oxygen deposited at 1×10^{-7} Torr for 5 min produced an ice thickness of 3.5 μm when an integrated absorption constant of 5×10^{-21} cm $molecule^{-1}$ is used. Taking into account the time and partial pressure, we estimated that the column density of $^{18}O_2$ within the sample is about 1.6×10^{18} molecules cm^{-2}, i.e. a thickness of around 554 nm. In deriving the column density of carbon monoxide, we used the overtone band at 4250 cm^{-1} because it can easily be monitored during the irradiation. Here, taking an absorption coefficient of 1.6×10^{-19} cm $molecule^{-1}$ (Gerakines et al. 2005), we derived a column density of $2.71 \pm 0.09 \times 10^{17}$ molecules cm^{-2}, i.e. a thickness of around 122 nm. Thus, the determined ratio of carbon monoxide to the isotopically labeled molecular oxygen is roughly 1:6; the total thickness is around 676 nm. The sample was then irradiated using 5 keV electrons generated by an electron gun (Specs EQ 22) for 1 hr at a beam current of 100 nA over a sample area of 1.8 ± 0.3 cm^2, noting that the manufacturer states an electron extraction efficiency of 78.8%. The sample was then left isothermally at 10 K for 80 min to check the stability and reactivity of the molecular species generated within the ice sample before the sample was heated to 300 K by a controlled heating program at a rate of 0.5 K min^{-1}.

Table 1
Species Identified in the Infrared Spectrum of the CO:$^{18}O_2$ Ice Prior to Irradiation

Band Position	Assignment	Characterization
4250	CO ($2\nu_1$)	Overtone band
3706	CO_2 ($\nu_1 + \nu_3$)	Combination band
3600	CO_2 ($2\nu_2 + \nu_3$)	Combination band
2346	CO_2 (ν_3)	Asymmetric stretch
2329	^{18}OCO (ν_3)	Isotope peak
2280	$^{13}CO_2$ (ν_3)	Isotope peak
2200br	CO ($\nu_1 + \nu_L$)	Fundamental + lattice mode
2137	CO (ν_1)	Fundamental
2111	CO–Ag (ν_1)	Fundamental
2092	^{13}CO (ν_1)	Isotope peak
2089	$C^{18}O$ (ν_1)	Isotope peak
2035br	...	...
2027	...	...
2002	...	...
1995	...	...
1485	$^{18}O_2$ ν_1	Fundamental
659, 646, 618	CO_2 ν_2	In-plane/out-of-plane bend
539	...	...

Note. "br" indicates a broad feature.

3. RESULTS

3.1. Infrared Spectroscopy

The infrared spectra of the CO:$^{18}O_2$ ices prior to the irradiation are shown in Figure 1 (gray line); the absorptions are listed in Table 1. The fundamental of the carbon monoxide species is found at 2137 cm^{-1}, in good agreement to studies where it has been studied within oxygen matrices (Ehrenfreund et al. 1996; Minenko et al. 2000). Other features, such as the broad lattice band centered around 2200 cm^{-1}, the overtone band at 4250 cm^{-1}, and an absorption band attributed to the formation of silver adsorbed carbon monoxide at 2111 cm^{-1} have all been discussed previously (Jamieson et al. 2006a). Two bands associated with the ^{13}CO and $^{12}C^{18}O$ isotopomers of carbon monoxide are characterized by their fundamental absorptions at 2092 and 2089 cm^{-1}, respectively. Again, these are in good agreement with the absorptions of these species isolated in argon matrices where they appear at 2091 and 2087 cm^{-1} (Schriver et al. 1999). Although it is infrared inactive, the fundamental of molecular oxygen ($^{18}O_2$) was observed at 1485 cm^{-1}, which is in agreement to previous studies (Jones et al. 1986). Carbon dioxide was also found in trace quantities, identified through its absorption bands at 618–659 (ν_2), 2346 (ν_3), 3706 ($\nu_1 + \nu_3$), and 3600 ($2\nu_2 + \nu_3$) cm^{-1}, respectively (Sandford & Allamandola 1990; Bennett et al. 2004); this originated from the carbon monoxide gas (99.9999%). Two more bands associated with the isotopomers of carbon dioxide, ^{18}OCO and $^{13}CO_2$ were identified through their ν_3 asymmetric stretches at 2329 and 2280 cm^{-1}, respectively (Cahill 1977). Also present in the spectrum are five unidentified bands, which appear at 2035, 2027, 2002, 1995, and 539 cm^{-1}. As none of these bands were present in our experiments with either pure carbon monoxide or the isotopically labeled molecular oxygen ices, it is postulated that they might be associated with complexes between the two molecules, possibly involving the silver surface.

Figure 1 (black line) also shows the infrared spectrum of the ice sample after the irradiation; the assigned peaks are compiled in Table 2. We shall first discuss briefly the effects of irradiation on the carbon monoxide bands; although a notable decrease in

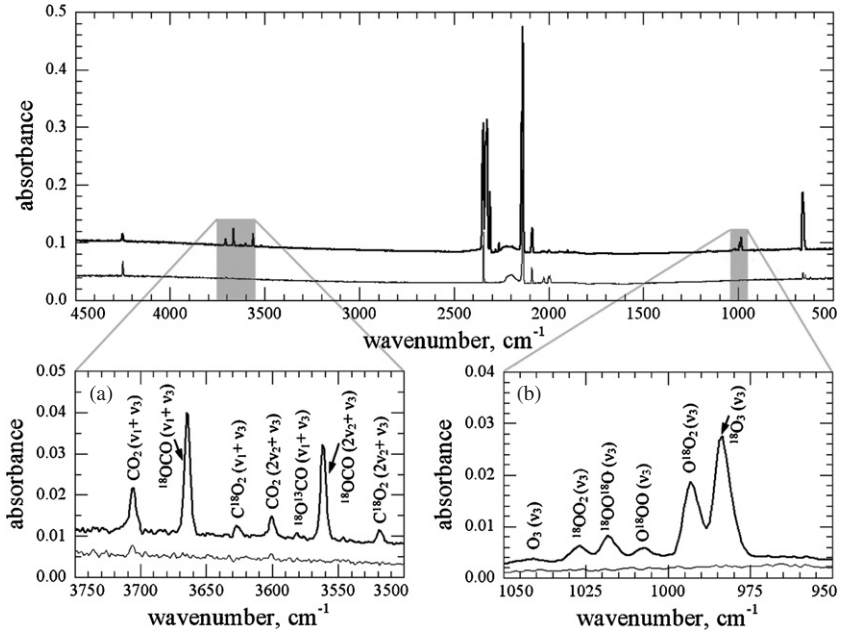

Figure 1. Infrared spectra over the range of 500–4500 cm^{-1} of the CO:$^{18}O_2$ ice held at 10 K prior to irradiation (gray) and after being subjected to 100 nA of 5 keV electrons for 1 hour (black). Inset (a) shows the region 3500–3750 cm^{-1} expanded to highlight the relative amounts of the combination bands of the observed carbon dioxide isotopomers. Similarly, inset (b) shows the ν_3 asymmetric stretching mode of the observed ozone bands within the region 950–1050 cm^{-1}.

the intensity of the overtone band at 4250 cm^{-1} is observed upon irradiation as it is destroyed while the fundamental band at 2137 cm^{-1} broadens slightly upon irradiation, as previously noted (Palumbo & Strazzulla 1993; Jamieson et al. 2006a). Deconvolution of this band reveals that this is due to the formation of a CO:CO_2 complex which produces two shoulder bands at 2144 and 2135 cm^{-1}, where they have previously been identified at 2143 and 2135 cm^{-1} (Raducu et al. 1995). An additional shoulder at 2140 cm^{-1} appears to be associated with a CO:O_3 complex, which again agrees to prior studies on this complex at 2140 cm^{-1} (Raducu et al. 1994). As expected, the ^{13}CO fundamental at 2092 cm^{-1} is found to decrease upon irradiation, while the $C^{18}O$ isotopomer at 2089 cm^{-1} grows.

The production of carbon dioxide during irradiation could clearly be seen. The ^{18}OCO isotopomer was shown to be the most abundant isotopomer produced, where new absorptions can be seen through the combination bands at 3665 (ν_1+ ν_3) and 3561 ($2\nu_2$+ ν_3). The $C^{18}O_2$ isotopomer could be identified through its ν_3 fundamental at 2311 cm^{-1} and its combination bands at 3626 (ν_1+ ν_3) and 3518 ($2\nu_2$+ ν_3) could also be clearly identified (Berney & Eggers 1964; Cahill 1977; Toth et al. 2007). In addition, bands due to $^{18}O^{13}CO$ at 3581 (ν_1+ ν_3), 3490 ($2\nu_2$+ ν_3), and 2263 (ν_3) were observed (Berney & Eggers 1964; Cahill 1977; Toth et al. 2008). A band at 2245 cm^{-1} is assigned to the ν_3 fundamental of $^{13}C^{18}O_2$ (Berney & Eggers 1964; Cahill 1977; Toth et al. 2008). Note that the additional band structure of the ν_3 isotopomers as listed in Table 2 is likely due to the formation of various Van der Waals complexes with different species within the matrix; however, their nature was not further investigated. The relative abundances of the different carbon dioxide isotopomers can be seen in Figure 1(a).

Considering the identification of ozone, the most abundant isotopomer was established to be $^{18}O_3$ which was found to lie in its most stable bent (C_{2v}) geometry, where the bands at 663 (ν_2), and 985 (ν_3) cm^{-1} are in good agreement with the values for this species within an oxygen matrix where they are found to occur at 664 and 982/984 cm^{-1}, respectively (Schriver-Mazzuoli et al. 1995). We also searched for evidence of the metastable cyclic (D_{3h}) isomer of this species, where theoretical calculations by Qu et al. (2005) predict that the most intense band should lie around 747 cm^{-1}, but were unable to find any trace of this species; all forms of ozone found were in their bent geometries. All six different isotopomers of ozone could be identified through their asymmetric stretching mode (ν_3), as depicted in Figure 1(b). Here, the other isotopomers, $O^{18}O_2$, $^{18}OO^{18}O$, $O^{18}OO$, $^{18}OO_2$, and O_3 were found to absorb at 994, 1018, 1007, 1027, and 1041 cm^{-1}, respectively, in good agreement with previous studies where they were found to lie at 992/993, 1017/1019, 1007/1008, 1026/1027, and 1040/1041 cm^{-1}, respectively (Schriver-Mazzuoli et al. 1995). The band occurring at 1712/1722 cm^{-1} was assigned to the (ν_2 + ν_3) band of indistinguishable isotopomers of ozone (Brewer & Wang 1972).

While they are not the subject of this investigation, a brief mention of other carbon oxide species found after irradiation should be made. Several different isotopomers of the $CO_3(C_{2v})$ and $CO_3(D_{3h})$ molecules can be identified (Table 2). These absorptions agree very well with previous measurements (Bennett et al. 2004; Jamieson et al. 2006b, 2007a). The $CO_4(C_{2v})$, $CO_5(C_2)$, and $CO_6(C_s)$ molecules could also be identified (Jamieson et al. 2007a, 2007b, 2008).

3.2. Mass Spectrometry

The majority of the matrix sublimes within the range of 23–43 K, in two overlapping episodes. The first maximum corresponds to carbon monoxide sublimation monitored via the CO^+ ion ($m/z = 28$) which peaks at 32 K (compared to 31 K for pure carbon monoxide; Jamieson et al. 2006a). The second peak is predominantly molecular oxygen, traced through the $^{18}O_2^+$ ion ($m/z = 36$) whereby a maximum was found at 37 K (found to be 38 K for pure molecular oxygen; Bennett & Kaiser 2005). Concurrent signals corresponding to the isotopomers of both carbon monoxide, $C^{18}O^+$ ($m/z = 30$) and molecular oxygen formed during irradiation, $^{16}O_2^+$ ($m/z = 32$) and $^{18}O^{16}O^+$

Table 2
Identification of Bands from New Species Formed During the Irradiation of the CO:$^{18}O_2$ Ice Sample at 10 K

Band Position	Assignment	Characterization
3706[a]	CO_2 (ν_1+ ν_3)	Combination band
3665	^{18}OCO (ν_1+ ν_3)	Isotope peak
3626	$C^{18}O_2$ (ν_1+ ν_3)	Isotope peak
3600[a]	CO_2 ($2\nu_2$+ ν_3)	Combination band
3581	$^{18}O^{13}CO$ (ν_1+ ν_3)	Isotope peak
3561	^{18}OCO ($2\nu_2$+ ν_3)	Isotope peak
3518	$C^{18}O_2$ ($2\nu_2$+ ν_3)	Isotope peak
3490	$^{18}O^{13}CO$ ($2\nu_2$+ ν_3)	Isotope peak
2351, 2346[a]	CO_2 (ν_3)	Asymmetric stretch
2336, 2329[a], 2325	^{18}OCO (ν_3)	Isotope peak
2311	$C^{18}O_2$ (ν_3)	Isotope peak
2280[a]	$^{13}CO_2$ (ν_3)	Isotope peak
	Carbon oxides	...
2263	$^{18}O^{13}CO$ (ν_3)	Isotope peak
2245	$^{13}C^{18}O_2$ (ν_3)	Isotope peak
2254, 2250, 2239, 2230, 2222, 2192	Carbon oxides	...
2144, 2140, 2137[a], 2135	CO (ν_1)	Fundamental
2109[a]	CO–Ag (ν_1)	Fundamental
2092[a]	Isotope peak	^{13}CO (ν_1)
2089[a]	Isotope peak	$C^{18}O$ (ν_1)
2066, 2060	Carbon oxides	...
2044, 2040, 2027, 2014	$C^{16/18}O_3$ (C_{2v}; ν_1)	Fundamental
2036, 2032	Carbon oxides	...
2002[a]	...	...
1995[a]	...	...
1947, 1943, 1932	$O = C^{16/18}O_3$ (C_{2v}; ν_1)	Fundamental
	$C_2{}^{18}O$ (ν_1)[b]	Fundamental
1927, 1922	Carbon oxides	...
1912	$O = C^{16/18}O_4$ (C_2; ν_1)	Fundamental
1906, 1900	$^{18}O = C^{16/18}O_3$ (C_{2v}; ν_1)	Fundamental
1871	$^{18}O = C^{16/18}O_4$ (C_2; ν_1)	Fundamental
	CO_3 (C_{2v}; Fermi)	Fermi resonance
	$O = CO_5$ (Cs; ν_1)	Fundamental
1863, 1856, 1842, 1832	$C^{16/18}O_3$ (C_{2v}, Fermi)	Fermi resonance
	$^{18}O = C^{16/18}O_5$ (Cs; ν_1)	Fundamental
1822	Carbon oxides	...
1712, 1722	$^{16/18}O_3$ (ν_2 + ν_3)	Combination band
1598	Carbon oxides	...
1545[b]	$^{16}O_2$ (ν_1)	Isotope peak
1485[a]	$^{18}O_2$ (ν_1)	Fundamental
1357, 1253, 1227, 1182	Carbon oxides	...
1171	CO_3 ($D_{3h;}$ ν_1)	Fundamental
1160	$^{16}OC^{18}O_2$ ($D_{3h;}$ ν_1)	Fundamental
1146	$^{16}OC^{18}O_2$ ($D_{3h;}$ ν_2)	Fundamental
1130, 1124	Carbon oxides	...
1065	$C^{16/18}O_3$ (C_{2v}; ν_2)	Fundamental
1041	O_3 (ν_3)	Isotope peak
1027	$^{18}OO_2$ (ν_3)	Isotope peak
1018	$^{18}OO^{18}O$ (ν_3)	Isotope peak
1007	$O^{18}OO$ (ν_3)	Isotope peak
994	$O^{18}O_2$ (ν_3)	Isotope peak
985	$^{18}O_3$ (ν_3)	Fundamental
1000, 830	Carbon oxides	...
681	$^{16/18}O_3$ (ν_2)	Isotope peak
663	$^{18}O_3$ (ν_2)	Fundamental
659[a], 647[a], 651, 633, 618[a]	$C^{16/18}O_2$ (ν_2)	Fundamental
576, 567, 554, 540	$C^{16/18}O_3$ (C_{2v}; ν_5)	Fundamental
521[b]	...	...

Notes. [a] These bands were present in the sample prior to irradiation. [b] Tentative detection. "Carbon oxides" refers to bands believed to be associated with C_xO_y ($x \geqslant 1$, $y \geqslant 1$) species which could not be specifically determined.

($m/z = 34$), were also detected. Although the majority of the ozone isotopomers were found to sublime with the bulk of the ice from 23 to 43 K, a later sublimation event occurred between 59 and 69 K, with a maximum at 62 K. Here, the signal

was attributed to the isotopomers of ozone as $^{18}O_3^+$ ($m/z = 54$) and $^{16}O^{18}O_2^+$ ($m/z = 52$). The last molecule identified as it sublimated from the ice was carbon dioxide over the period of 76–90 K (maximum signal recorded around 89 K), again in good agreement with previous studies (91–94 K; Bennett et al. 2004). Here, the signals from carbon dioxide were monitored at CO_2^+ ($m/z = 44$), $^{18}OCO^+$ ($m/z = 46$), and $C^{18}O_2^+$ ($m/z = 48$).

4. DISCUSSION

4.1. Formation of Ozone

As molecular oxygen is the dominant chemical species within our ice mixture, let us first consider the formation of ozone; the only observed product when pure ices are subjected to keV electrons (Bennett et al. 2005). The temporal profile of the $^{18}O_3$ isotopomer of ozone was taken from the ν_3 asymmetric stretch found at 985 cm^{-1}; the absorption coefficient of 1.4×10^{-17} cm molecule^{-1} for this band was used for all isotopomers (Smith et al. 1985). Our previous work showed that the formation of ozone followed pseudo-first-order kinetics. Formerly, the radiolysis induced bond cleavage within molecular oxygen generates free suprathermal oxygen atoms, which then react with neighboring molecular oxygen (in excess) to generate ozone as depicted in reaction (8)

$$[^{18}O_2 \ldots {}^{18}O_2] \xrightarrow{k_1} [^{18}O \ldots {}^{18}O \ldots {}^{18}O_2] \xrightarrow{\text{fast}} [^{18}O \ldots {}^{18}O_3]. \quad (8)$$

Note that the addition of an oxygen atom to form the bent (C_{2v}) ozone structure requires passing a barrier of only around 100 cm^{-1} (144 K; 1 kJ mol^{-1}; Schinke & Fleurat-Lessard 2004). This justifies fitting the temporal profiles using pseudo-first-order kinetics, as the reaction will occur rapidly with suprathermal oxygen atoms. Conversely, in the 6:1 (O_2:CO) ice, we observe a decrease in the observed column density, indicating that ozone is either reacting with other chemical species present within the ice, or being dissociated by the impinging electrons. Dissociation is likely to generate molecular oxygen and suprathermal oxygen atoms; in the case of pure molecular ices it is anticipated that this will ultimately cause the regeneration of a second ozone molecule, indiscernible from the original. However, within mixed ices, these oxygen atoms can be intercepted by other chemical species, here labeled simply as X:

$$[^{18}O_2 \ldots {}^{18}O_2 \ldots X] \xrightarrow{k_1} [^{18}O \ldots {}^{18}O_3 \ldots X] \xrightarrow{k_2} [^{18}O \ldots {}^{18}O_2 \ldots {}^{18}OX] \quad (9)$$

for which we obtain the following rate equation (Steinfeld et al. 1999):

$$[^{18}O_3]_t = \frac{k_1 a}{k_2 - k_1}(e^{-k_1 t} - e^{-k_2 t}). \quad (10)$$

Here, we find that $a = 4.18 \pm 0.03 \times 10^{15}$ molecules cm^{-2}, $k_1 = 1.44 \pm 0.02 \times 10^{-3}$ s^{-1}, and $k_2 = 9.35 \pm 0.36 \times 10^{-5}$ s^{-1}; the results are shown in Figure 2(a). As a consequence of the low barrier involved in the generation of ozone, it is anticipated that if free oxygen ^{16}O atoms are available as generated through reaction (5), the temporal profile of the $O^{18}O_2$ isotopomer should be consistent with these findings. The proposed reaction sequence is shown below:

$$[CO \ldots {}^{18}O_2] \xrightarrow{k_3} [C \ldots O \ldots {}^{18}O_2] \xrightarrow{\text{fast}} [C \ldots O^{18}O_2]. \quad (11)$$

Here, the temporal profile should be fit via pseudo-first-order kinetics:

$$[O^{18}O_2]_t = b(1 - e^{-k_3 t}), \quad (12)$$

where the results of the fit (shown in Figure 2(b)) give $b = 1.93 \pm 0.01 \times 10^{15}$ molecules cm^{-2} and $k_3 = 1.08 \pm 0.01 \times 10^{-3}$ s^{-1}. The rate constant is of the same order as that found for the $^{18}O_3$ isotopomer, although we should bear in mind it is likely that a small proportion of this isotopomer is being destroyed in accordance with the previous result, although at a rate below the sensitivity of our analysis.

It is interesting that we were also able to fit the temporal profile of the $^{18}OO^{18}O$ isotopomer of ozone, which was produced from the ν_3 asymmetric stretch at 1018 cm^{-1}, using pseudo-first-order kinetics as follows:

$$[^{18}OO^{18}O]_t = c(1 - e^{-k_4 t}). \quad (13)$$

The results of this fit being, $c = 7.81 \pm 0.40 \times 10^{14}$ molecules cm^{-2} and $k_4 = 4.02 \pm 0.34 \times 10^{-4}$ s^{-1}. The fit is shown in Figure 2(c). The lower rate constant could be interpreted found here could be explained by a lower reactive cross section for the "insertion" of the oxygen ^{16}O atom into the molecular oxygen which would have a lower cone of acceptance compared to adding to a terminal atom. However, theoretical calculation by Siebert et al. (2002) shows that the direct insertion process does not occur, indicating the possible involvement of a cyclic intermediate which can subsequently ring open to form this isotopomer. Instead, these calculations suggest that the ^{16}O atom must add to a terminal oxygen atom initially, and then may transiently form the cyclic species (overcoming a barrier of around 1.3 eV (15,086 K; 125 kJ mol^{-1})) before ring opening to form the $^{18}OO^{18}O$ isotopomer.

4.2. Formation of Carbon Dioxide

Here, considering we have already established the presence of free suprathermal ^{18}O atoms within our ice, we should initially consider their reaction with carbon monoxide to form the ^{18}OCO isotopomer of carbon monoxide. The temporal profile for this species was produced from monitoring the ν_3 asymmetric stretch at 2329 cm^{-1}, using the integrated absorption coefficient of 7.6×10^{-17} cm molecule^{-1} (Gerakines et al. 1995). During irradiation, two shoulder bands at 2336 and 2325 cm^{-1} become apparent, causing artificially large error bars due to nonunique solutions within the deconvolution procedure. These are likely associated with complexes between ^{18}OCO with CO and/or O_3. The proposed reaction is

$$[CO \ldots {}^{18}O_2] \xrightarrow{k_5} [CO \ldots {}^{18}O \ldots {}^{18}O] \xrightarrow{\text{fast}} [OC^{18}O \ldots {}^{18}O], \quad (14)$$

where the temporal profile should be fit by

$$[^{18}OCO]_t = d(1 - e^{-k_5 t}) \quad (15)$$

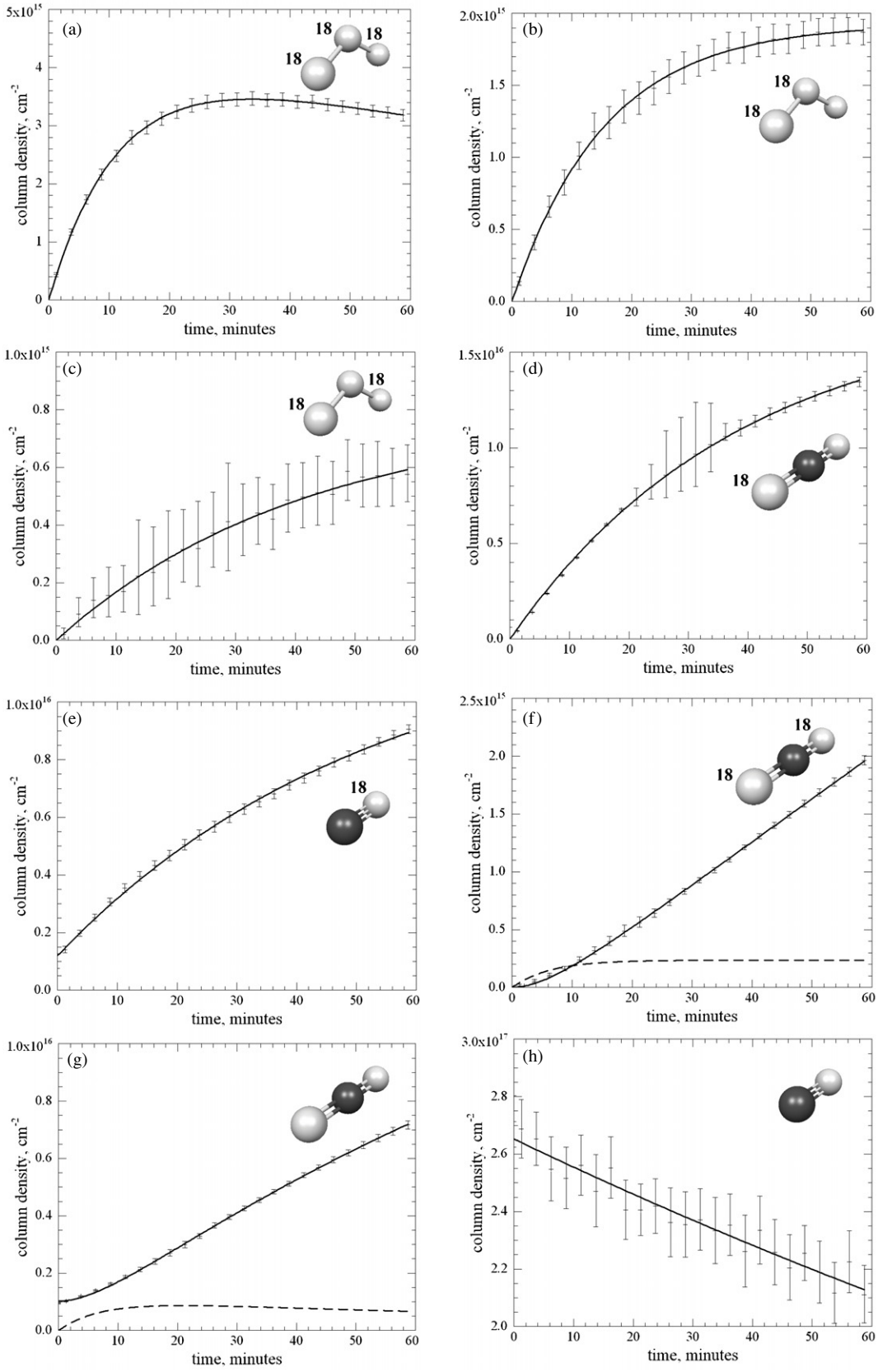

Figure 2. Kinetic fits to the temporal profiles of the column densities during the irradiation period for (a) $^{18}O_3$, (b) $O^{18}O_2$, (c) $^{18}OO^{18}O$, (d) ^{18}OCO, (e) $C^{18}O$, (f) $C^{18}O_2$, (g) CO_2, and (h) CO (see for details).

the results were found to be $d = 1.73 \pm 0.02 \times 10^{16}$ molecules cm^{-2}, and $k_5 = 4.31 \pm 0.08 \times 10^{-4}$ s^{-1}, and are shown in Figure 2(d). This is consistent with the theoretical calculations of Talbi et al. (2006) as the suprathermal oxygen atoms are able to overcome the barrier to this reaction. Note that we cannot exclude the involvement of excited $^{18}O(^1D)$ oxygen atoms which can react without barrier to form carbon dioxide.

The production of the $C^{18}O_2$ isotopomer was investigated to discern whether or not there was evidence for the reaction of free suprathermal carbon atoms with molecular oxygen. Here, the theoretical calculations of Hwang & Mebel (2000) predict that this pathway is feasible, passing through both linear and cyclic intermediates. The temporal profile was produced from the ν_3 asymmetric stretch at 2311 cm^{-1}. We were unable to identify these intermediates, and in addition, the profile for this species is not consistent with this mechanism. Instead, we propose that this molecule can be produced in a two-step sequential mechanism whereby it is most likely that the initial step is the generation of the $C^{18}O$ species, and its production must be accounted for before further investigation into the formation of $C^{18}O_2$. Here, there are three main pathways to consider: (1) the recombination of atomic carbon and oxygen atoms, (2) the isotopic exchange reaction from reaction of suprathermal ^{18}O atoms with carbon monoxide as investigated by Brunsvold et al. (2008) to be relatively inefficient, and (3) the reaction of carbon atoms with molecular oxygen. This process is found to occur rapidly, even at low temperatures as studied by Chastaing et al. (2000). Investigations by Geppert et al. (2002) indicate that the process can occur without barrier, and produces carbon monoxide and an electronically excited oxygen atom. We consider this the most likely pathway, which is depicted as follows:

$$[^{18}O_2 \ldots CO] \xrightarrow{k_6} [^{18}O_2 \ldots C \ldots O] \xrightarrow{\text{fast}} [^{18}O \ldots C^{18}O \ldots O]. \quad (16)$$

The temporal profile for this species was produced from the ν_1 fundamental occurring at 2089 cm^{-1} with the absorption coefficient of 1.1×10^{-17} cm molecule^{-1} (Jiang et al. 1975). Here, the kinetic fit used is given as

$$[C^{18}O]_t = f(1 - e^{-k_6 t}). \quad (17)$$

From the results, we find $f = 1.58 \pm 0.03 \times 10^{16}$ molecules cm^{-2} and $k_6 = 3.14 \pm 0.16 \times 10^{-4}$ s^{-1}. The results can be seen in Figure 2(e); note that due to the presence of this isotopomer prior to irradiation, an additional column density of $1.19 \pm 0.05 \times 10^{15}$ molecules cm^{-2} was added as a constant to Equation (17). Now, we can return to the proposed two-step formation of $C^{18}O_2$, which may form via the addition of a suprathermal ^{18}O atom to a previously generated $C^{18}O$ molecule:

$$[CO \ldots {}^{18}O_2] \xrightarrow{k_7} [O \ldots {}^{18}OC \ldots {}^{18}O] \xrightarrow{k_8} [O \ldots C^{18}O_2]. \quad (18)$$

Now, the temporal profile can be fit using the following kinetic equation:

$$[C^{18}O_2]_t = g\left(1 - \frac{k_8}{k_8 - k_7} e^{-k_7 t} + \frac{k_7}{k_8 - k_7} e^{-k_8 t}\right). \quad (19)$$

For this isotopomer, it was necessary to fix the value of $g = 1.70 \times 10^{16}$ molecules cm^{-2}; using this value, we determined $k_7 = 3.89 \pm 0.03 \times 10^{-5}$ s^{-1}, and $k_8 = 2.23 \pm 0.08 \times 10^{-3}$ s^{-1}. The results are depicted in Figure 2(f); the dashed line shown indicates the required column density of $C^{18}O$ molecules necessary to make this pathway feasible.

Finally, for the CO_2 isotopomer of carbon dioxide, we expect that the ratio of our ice mixture discriminates against the likelihood of reactions (6) and (7) occurring to any great extent, similar to the observations by Cottin et al. (2003). This is verified by the temporal profile, which cannot be fitted by first-order kinetics. Here, we assumed that an initially generated ^{16}O atom would have to react via an intermediately generated species, following pseudo-first-order kinetics, and then the process may be repeated to generate the carbon dioxide molecule:

$$[CO \ldots X \ldots CO] \xrightarrow{k_9} [C \ldots OX \ldots CO] \xrightarrow{k_{10}} [C \ldots X \ldots CO_2]. \quad (20)$$

Again, this profile can be fitted using a two-step sequential mechanism via

$$[CO_2]_t = h\left(1 - \frac{k_{10}}{k_{10} - k_9} e^{-k_9 t} + \frac{k_9}{k_{10} - k_9} e^{-k_{10} t}\right). \quad (21)$$

The results are shown in Figure 2(g); here, we find that $h = 1.73 \pm 0.19 \times 10^{16}$ molecules cm^{-2}, $k_9 = 1.42 \pm 0.20 \times 10^{-4}$ s^{-1}, and $k_{10} = 2.38 \pm 0.21 \times 10^{-3}$ s^{-1}. Note due to the presence of a small amount of the CO_2 in the sample prior to irradiation, a constant of $1.03 \pm 0.02 \times 10^{15}$ molecules cm^{-2} was added as a constant to Equation (21). The amount of species X required to participate in this reaction sequence to make it feasible is indicated by the dotted line.

4.3. Destruction of Carbon Monoxide

The 1:6 ratio within our ice matrix lessens the extent of reactions (6) and (7) occurring as a reaction pathway to destroy carbon monoxide, as has been previously commented. If this were the major destruction pathway, we would expect to see the first order generation of carbon dioxide so we can safely assume that this pathway is not a dominant destruction pathway, but may occur to a small extent. In the previous two sections, we verified the first-order production of species dependant upon the generation of both free suprathermal ^{16}O (reactions (11)–(13)) and C atoms (reactions (16)–(17)). This seems to verify that reaction (5), the radiolysis-induced dissociation of carbon monoxide, takes place within our ice matrix. However, we still cannot assume that reaction (5) is solely responsible for the destruction of this species. In fact, we have already postulated that reactions (14) and (20), the addition of suprathermal $^{16/18}O$ atoms to carbon monoxide to form the CO_2 and ^{18}OCO isotopomers of carbon dioxide, will attribute to the destruction process. The destruction of carbon monoxide was monitored via the $2\nu_1$ overtone band at 4250 cm^{-1}, whereby the absorption coefficient of 1.6×10^{-19} cm molecule^{-1} was used to derive the column density (Gerakines et al. 2005). In consideration of the destruction pathways for this molecule, the column density was fitted using an exponential decay, whereby the major contributing pathway is expected to be reaction (5).

$$[CO]_t = [CO]_0 e^{-k_{11} t}. \quad (22)$$

Here $[CO]_t$ is the column density at time t, and $[CO]_0$ is the initial column density of carbon monoxide. The results from the fit are depicted in Figure 2(h), where $[CO]_0 = 2.65 \pm 0.02 \times 10^{17}$ molecules cm^{-2} and $k_{11} = 6.24 \pm 0.34 \times 10^{-5}$ s^{-1}.

4.4. Astrophysical Implications

From an astrophysical perspective, the ice environment studied here may be typical of that of interstellar ices where the carbon monoxide is found within an apolar ice which is identified through a narrow feature at 2140 cm^{-1}. Here, the dominant species expected to be constituents of the surrounding matrix are thought to be carbon monoxide itself, molecular nitrogen, molecular oxygen, and carbon dioxide, which is also found in these environments (Tielens et al. 1991; Chiar et al. 1994, 1995). Whereas carbon monoxide, molecular oxygen and molecular nitrogen all have similar volatilities, carbon dioxide is much less volatile, so its presence in such an environment is possible evidence for its formation there through the processing of these ices. It has been previously mentioned that many of the astronomical environments where this processing through radiolysis is proposed to occur are actually thought to be quiescent environments which are not significantly processed by UV photons such as Elias 16 (Nummelin et al. 2001) and the dark clouds of the Orion core (Whittet et al. 2007). However, it is well known that the galactic cosmic radiation (GCR) can penetrate even within these dark clouds. Here, the particle component consists of around 98% protons, and 2% helium nuclei (α-particles) which have an energy distribution maximum around 10 MeV, where a fluence of $\phi = 10$ particles cm^{-2} s^{-1} (Strazzulla & Johnson 1991). However, the generation of such high-energy particles is quite difficult and although such experiments have been carried out using particles generated by a cyclotron (Kaiser & Roessler 1997; Kaiser et al. 1997), it is more customary to use lower energy particles typically of around 0.8 MeV generated with a van de Graaff generator (e.g., Gerakines & Moore 2001). The linear energy transfer (LET) is an indicator of how much energy is transferred into the medium as a particle transverses the medium, and is directly related to the distribution of excited particles; it explains why different chemical yields can be observed for different energy ranges (Swallow 1973; Magee & Chatterjee 1987; Johnson 1990; Spinks & Woods 1990). Thus, while the LET for a 10 MeV proton in carbon monoxide has been calculated to be 4.1 keV μm^{-1}, a 0.8 MeV proton has an LET of 21.1 keV μm^{-1}, as calculated using the SRIM code (Ziegler et al. 1985). This energy deposition is split between two different types of collisions; elastic nuclear collisions (S_n) and inelastic electronic collisions (S_e). While elastic nuclear collisions can transfer large amounts of energy to generate knock-on particles which may carry up to 10 keV of kinetic energy, they are sparsely generated, typically several μm apart (Kaiser & Roessler 1997; Kaiser et al. 1997; Magee & Chatterjee 1987). In fact, Monte Carlo simulations of ion trajectories using both the SRIM and MARLOWE codes indicate that a 10 MeV proton typically loses over 99.9% of its energy through elastic electronic collisions (Ziegler et al. 1985; Kaiser & Roessler 1997; Kaiser et al. 1997). These elastic electronic collisions refer to the excitation of electrons through interaction with the incoming charged particle; if the extent of excitation is large enough it will create an ionized species and a secondary electron (δ electrons), otherwise this energy may be internally dissipated into electronic, vibrational, and rotational energy levels. Recall that if a dissociative electronic state is involved, the bond may rupture to generate radical species. During these interactions, it is the speed of the charged particle as it transverses a molecule which is important because the timescale the electrons within the medium have to react to their influence is important (Magee & Chatterjee 1987). The speed of a 10 MeV proton is similar to that of a 5 keV electron, which explains why their LET is similar; the values often reported for a 5 keV electron are close to 4 keV μm^{-1} as calculated by the CASINO code (Drouin et al. 2001). The only anticipated difference is in the energies of secondary electrons generated. While the energy of secondary electrons released from a 10 MeV proton track can be generated with up to a few 10^4 eV, compared to around 2500 eV as an upper limit for the electrons generated via 5 keV electrons, where there is an inverse square relationship to the likelihood of generating higher energy particles (Magee & Chatterjee 1987). Thus, here we are directly investigating the effects of the δ electrons, in an energy regime where the effects should be comparable to that of a 10 MeV proton. While elastic nuclear interactions, as well as charge transfer, and even these ions reacting themselves with the target medium become increasingly important considerations in ion implantation at lower energies, it is safe to neglect them within this energy range (Swallow 1973; Magee & Chatterjee 1987; Johnson 1990; Spinks & Woods 1990).

There is a large amount of evidence supporting the fact that carbon monoxide is found not only within apolar ices, but can also be trapped within water-dominated regions of interstellar grains (Chiar et al. 1994, 1995; Collings et al. 2003). When mixtures of H_2O:CO ices are exposed to UV radiation or energetic ions, the production of carbon dioxide is readily observed (Moore et al. 1991; Watanabe & Kouchi 2002). This helps explain recent observations by Whittet et al. (2009), where the spectral features of the carbon dioxide bands indicate that even for dense molecular clouds, up to 85% of this molecule reside within a polar (water dominated) matrix. This is surprising given the fact that carbon dioxide seems more likely to form within the nonpolar regions which are dominated by CO, O_2, and N_2. One possible explanation for this seemingly paradoxical observation is that as we have shown here, carbon dioxide can be formed from carbon monoxide *wherever* there is a source of suprathermal oxygen atoms. These can be donated from *any* oxygen-bearing species to generate carbon dioxide, although here, the donor is most likely water. In this case, the left-over hydrogen atoms are free to diffuse within these porous ices. They may eventually recombine to form molecular hydrogen which may be released from the ice, or react with other constituents of the ice. However, as the concentration of carbon dioxide within these ices without any irradiation source is expected to be near zero, the relative amounts of CO:CO_2 *within the water dominated regions* of interstellar ices, could be an indicator for how much processing these ices have experienced, and may be linked to the concentrations of other species such as formaldehyde and methanol.

Note also that carbon dioxide can readily form within the apolar regions of interstellar ices, where carbon monoxide and oxygen are two of the three dominating species, very similar to the ices used here. It is anticipated that during the processing of such an ice, spectral features from ozone and carbon dioxide will become apparent. In addition, there may be shoulder bands on several of these features which are associated with van der Waals complexes. Recently, Pontoppidan et al. (2003) conducted a study where they reported spectral features associated with the

Table 3
Summary of Key Reactions Occurring Within the CO:$^{18}O_2$ Ice Matrix During the Irradiation

Initial Processes	(1) $^{18}O_2 \rightarrow {}^{18}O + {}^{18}O$
	(2) $CO \rightarrow C + O$
First generation products	(3) $^{18}O + {}^{18}O_2 \rightarrow {}^{18}O_3$
	(4) $^{18}O + CO \rightarrow {}^{18}OCO$
	(5) $O + {}^{18}O_2 \rightarrow O^{18}O_2$ ($\rightarrow {}^{18}OO^{18}O$)
	(6) $C + {}^{18}O_2 \rightarrow C^{18}O + {}^{18}O$
Secondary processes	(7) $^{18}O_3 \rightarrow {}^{18}O + {}^{18}O_2$
	(8) $O^{18}O_2 \rightarrow O^{18}O + {}^{18}O$
	$\rightarrow O + {}^{18}O_2$
	(9) $^{18}OO^{18}O \rightarrow O^{18}O + {}^{18}O$
	(10) $^{18}OCO \rightarrow C^{18}O + O$
	$\rightarrow CO + {}^{18}O$
Second generation products	(11) $CO + O \rightarrow CO_2$
	(12) $C^{18}O + {}^{18}O \rightarrow C^{18}O_2$

fundamental band of carbon monoxide in ices around young, low mass stars (which may still have significant amounts of apolar ices). They observed bands centered around 2143.7, 2139.9, and 2136.6 cm^{-1}, and commented that these spectral features were not consistent with carbon monoxide trapped within a polar matrix. It is suggested that these spectral features may be indicative of complexes between carbon monoxide and carbon dioxide (also, possibly ozone) where they have previously been recorded at 2144 and 2135 cm^{-1} (Raducu et al. 1996). Again, this may show evidence of the neighboring species to carbon monoxide and give clues to the amount of processing these ices have been subjected to.

5. CONCLUSION AND SUMMARY

This paper focused on the destruction of carbon monoxide and formation of carbon dioxide under the irradiation with energetic electrons; the subsequently isotopic variants were followed in order to extract the reaction mechanisms. The key reaction pathways identified here, occurring during the irradiation processes, are compiled in Table 1. The initial processes refer to the dissociation of the precursor molecules within the ice, and are verified by monitoring the temporal profiles of derived column densities for each of the first generation products that can be generated (Table 3), whereby each were found to be consistent with pseudo-first-order kinetics. Specifically, the generation of ^{18}O atoms from the dissociation of molecular oxygen is verified by the first-order generation of $^{18}O_3$ (as previously reported by Bennett et al. 2005), as well as ^{18}OCO. In a similar manner, the generation of C and O atoms by the dissociation of carbon monoxide through reaction (5) is verified by the first order production of $O^{18}O_2$, $^{18}OO^{18}O$, and $C^{18}O$. This pathway is not expected to occur when ices are subjected to UV photons. Here, it has been shown that instead of dissociation, the UV radiation causes the generation of electronically excited carbon monoxide molecules (reaction (6)), which can then react with neighboring molecules to generate carbon dioxide and a carbon atom (reaction (7)). Evidence for this mechanism is shown, by the fact that when carbon monoxide is diluted within a 10:1 nitrogen dominated matrix and irradiated by UV photons, carbon dioxide is not produced (Cottin et al. 2003).

During the irradiation of our ice, it is apparent that the first generation products are also dissociated during the irradiation. Though the only temporal profile for which this is clearly shown is for the $^{18}O_3$ isotopomer of ozone (Figure 2(a)), we expect that the radiation-induced dissociation of ^{18}OCO, $O^{18}O_2$, $^{18}OO^{18}O$, and $C^{18}O$ will occur to some extent. Table 3 lists some of the products likely to result from the processing of these first generation products. Here, we note that we have several new pathways for producing free suprathermal O atoms, as well as ^{18}OO. The release of suprathermal O atoms from these first generation products is in accordance with our proposed mechanisms for the two-step sequential process we indicated for the production of CO_2 within our ice sample. The further reaction of $C^{18}O$ with a second suprathermal ^{18}O atom to produce $C^{18}O_2$ is also consistent with our proposed mechanisms. Evidence for the presence of ^{18}OO in our sample comes from mass spectrometry, where we were able to observe signals corresponding to $^{18}OO^+$ ($m/z = 34$) as well as O_2^+ ($m/z = 32$) which sublimed along with $^{18}O_2$ during the warm-up of our ice. The latter represents further evidence for free O atoms available to recombine within our matrix; which would not be readily available if reactions (6) and (7) were solely responsible for the destruction of carbon monoxide.

We have also shown that the production of carbon dioxide from carbon monoxide reacting with suprathermal oxygen atoms is efficient. The fact that any oxygen bearing molecule residing within interstellar ices can produce suprathermal oxygen atoms when subjected to irradiation by MeV ions is stressed. This indicates that carbon dioxide can be produced from carbon monoxide both within the polar as well as apolar regions of interstellar ices. Most importantly, the decomposition and reactivity of carbon monoxide depends on the chemical environment of the interstellar ices. Upon exposure to energetic electrons, *isolated* carbon monoxide molecules are able to undergo unimolecular decomposition to give suprathermal carbon (C) and oxygen (O) atoms. Molecular oxygen decomposes to two oxygen atoms. The free oxygen atoms can react with carbon monoxide via addition to form the carbon dioxide isotopomers as observed experimentally. This mechanism to form carbon dioxide is distinctly different from the one observed in pure carbon monoxide ices in the *bulk* where electronically excited carbon monoxide reacts with a neighboring carbon monoxide molecule to form solely carbon dioxide and a carbon atom.

This material is based up work supported by the National Aeronautics Space Administration (NASA Astrobiology Institute under Cooperative Agreement no. NNA04CC08A issued through the Office of Space Science).

REFERENCES

Aikawa, Y., Ohashi, N., Inutsuka, S.-I., & Herbst, E. 2001, ApJ, 522, 639
Aikawa, Y., Wakelem, V., Garrod, R. T., & Herbst, E. 2008, ApJ, 674, 984
Baird, T. 1972, Carbon, 10, 723
Bakker, B. L. G., & Parker, D. H. 2000, Chem. Phys. Lett., 330, 293
Bennett, C. J., Jamieson, C., Mebel, A. M., & Kaiser, R. I. 2004, Phys. Chem. Chem. Phys., 6, 735
Bennett, C. J., Jamieson, C. S., Osamura, Y., & Kaiser, R. I. 2005, ApJ, 624, 1097
Bennett, C. J., & Kaiser, R. I. 2005, ApJ, 635, 1362
Berney, C. V., & Eggers, D. F. Jr. 1964, J. Chem. Phys., 40, 990
Boonman, A. M. S., van Dishoeck, E. F., Lahuis, F., & Doty, S. D. 2003, A&A, 399, 1063
Brewer, L., & Wang, J. L.-F. 1972, J. Chem. Phys., 56, 759
Brunsvold, A., Upadhyaya, H. P., Zhang, J., Cooper, R., Minton, T. K., Braunstein, M., & Duff, J. W. 2008, J. Phys. Chem. A, 112, 2192
Cahill, J. E. 1977, J. Chem. Phys., 66, 4847
Chastaing, D., Le Picard, S. D., & Sims, I. R. 2000, J. Chem. Phys., 112, 8466
Chiar, J. E., Adamson, A. J., Kerr, T. H., & Whittet, D. C. B. 1994, ApJ, 426, 240

Chiar, J. E., Adamson, A. J., Kerr, T. H., & Whittet, D. C. B. 1995, ApJ, 455, 234
Chrisey, D. B., Boring, J. W., Phipps, J. A., Johnson, R. E., & Brown, W. L. 1986, Nucl. Instrum. Methods Phys. Res., 13, 360
Collings, M. P., Dever, J. W., Fraser, H. J., McCoustra, M. R. S., & Williams, D. A. 2003, ApJ, 583, 1058
Cottin, H., Moore, M. H., & Bénilan, Y. 2003, ApJ, 590, 874
Dartois, E., Demyk, K., Gerin, M., & d'Hendecourt, L. 2000, in ISO Beyond the Peaks: The 2nd ISO Workshop on Analytical Spectroscopy (ESA-SP 456), ed. A. Salama, M. F. Kessler, K. Leech, & B. Schulz (Madrid: Villafranca del Castillo), 71
de Graauw, Th., et al. 1996, A&A, 315, L345
d'Hendecourt, L. B., & Jourdain de Muizon, M. 1989, A&A, 223, L5
Drouin, D., Couture, A. R., Gauvin, R., Hovington, P., Horny, P., & Demers, H. 2001, Monte Carlo Simulation of Electron Trajectory in Solids (CASINO), ver 2.42 (Sherbrooke: Univ. Sherbrooke)
Ehrenfreund, P., Boogert, A. C. A., Gerakines, P. A., Jansen, D. J., Schutte, W. A., Tielens, A. G. G. M., & van Dishoeck, E. F. 1996, A&A, 315, L341
Fournier, J., Deson, J., Vermeil, C., & Pimentel, G. C. 1979, J. Phys. Chem., 70, 5726
Geppert, W. D., Naulin, C., & Costes, M. 2002, Chem. Phys. Lett., 364, 121
Gerakines, P. A., Bray, J. J., Davis, A., & Richey, C. R. 2005, ApJ, 620, 1140
Gerakines, P. A., & Moore, M. H. 2001, Icarus, 154, 372
Gerakines, P. A., Schutte, W. A., & Ehrenfreund, P. 1996, A&A, 312, 289
Gerakines, P. A., Schutte, W. A., Greenberg, J. M., & van Dishoeck, E. F. 1995, A&A, 296, 810
Gibb, E. L., Whittet, D. C. B., Boogert, A. C. A., & Tielens, A. G. G. M. 2004, ApJS, 151, 35
Grim, R. J. A., & d'Hendecourt, L. B. 1986, A&A, 167, 161
Haring, R. A., Pedrys, R., Oostra, D. J., Haring, A., & De Vries, A. E. 1984, Nucl. Instrum. Methods Phys. Res., 5, 476
Hwang, D.-Y., & Mebel, A. M. 2000, Chem. Phys., 256, 169
Jamieson, C. S., Mebel, A. M., & Kaiser, R. I. 2006a, ApJS, 163, 184
Jamieson, C. S., Mebel, A. M., & Kaiser, R. I. 2006b, Chem. Phys. Chem., 7, 2508
Jamieson, C. S., Mebel, A. M., & Kaiser, R. I. 2007a, Chem. Phys. Lett., 443, 49
Jamieson, C. S., Mebel, A. M., & Kaiser, R. I. 2007b, Chem. Phys. Lett., 440, 105
Jamieson, C. S., Mebel, A. M., & Kaiser, R. I. 2008, Chem. Phys. Lett., 450, 312
Jiang, G. J., Person, W. B., & Brown, K. G. 1975, J. Chem. Phys., 62, 1201
Johnson, R. E. 1990, Energetic Charged Particle Interactions with Atmospheres and Surfaces (Springer: Berlin)
Jones, L. H., Agnew, S. F., Swanson, B. I., & Ekberg, S. A. 1986, J. Chem. Phys., 85, 428
Kaiser, R. I., Eich, G., Gabrysch, A., & Roessler, K. 1997, ApJ, 484, 487
Kaiser, R. I., & Roessler, K. 1997, ApJ, 475, 144
Loeffler, M. J., Baratta, G. A., Palumbo, M. E., Strazzulla, G., & Baragiola, R. A. 2005, A&A, 435, 587
Magee, J. L., & Chatterjee, A. 1987, in Radiation Chemistry: Principles and Applications, ed. Farhataziz & M. A. J. Rodgers (New York: VCH)
Martin, J.-P, Perrin, M.-Y., & Porshnev, P. I. 2000, Chem. Phys. Lett., 332, 283
Millar, T. J., Rawlings, J. M. C., Bennett, A., Brown, P. D., & Charnley, S. B. 1991, A&AS, 87, 585
Minenko, M., Vetter, M., Brodyanski, A. P., & Jodl, H. J. 2000, Low Temp. Phys., 26, 699
Moore, M. H., Khanna, R., & Donn, B. 1991, J. Geophys. Res., 96, 17541
Muñoz Caro, G. M., & Schutte, W. A. 2003, A&A, 412, 213
Nummelin, A., Whittet, D. C. B., Gibb, E. L., Gerakines, P. A., & Chiar, J. E. 2001, ApJ, 558, 185
Okabe, H. 1978, Photochemistry of Small Molecules (New York: Wiley)
Palumbo, M. E., & Strazzulla, G. 1993, A&A, 268, 568
Pontoppidan, K. M. 2006, A&A, 453, L47
Pontoppidan, K. M., et al. 2003, A&A, 408, 981
Qu, Z.-W., Zu, H., & Schinke, R. 2005, J. Chem. Phys., 123, 204324
Raducu, V., Gauthier-Roy, B., Dahoo, R., Abouaf-Margin, L., Langlet, J., Caillet, J., & Allavena, M. 1996, J. Chem. Phys., 105, 10092
Raducu, V., Jasmin, D., Dahoo, R., Brosset, P., Gauthier-Roy, B., & Abouaf-Marguin, L. 1994, J. Chem. Phys., 101, 1878
Raducu, V., Jasmin, D., Dahoo, R., Brosset, P., Gauthier-Roy, B., & Abouaf-Marguin, L. 1995, J. Chem. Phys., 102, 9235
Roser, J. E., Vidali, G., Manico, G., & Pirronello, V. 2001, ApJ, 555, L61
Ruffle, D. P., & Herbst, E. 2001, MNRAS, 324, 1054
Sandford, S. A., & Allamandola, L. J. 1990, ApJ, 355, 357
Schinke, R., & Fleurat-Lessard, P. 2004, J. Chem. Phys., 121, 5789
Schriver, A., Schriver-Mazzuoli, L., Chaquin, P., & Bahou, M. 1999, J. Phys. Chem. A, 103, 2624
Schriver-Mazzuoli, L., de Saxcé, A., Lugez, C., Camy-Peyret, C., & Schriver, A. 1995, J. Chem. Phys., 102, 690
Sheffer, Y., Rogers, M., Federman, S. R., Abel, N. P., Gredel, R., Lambert, D. L., & Shaw, G. 2008, ApJ, 687, 1075
Siebert, R., Fleurat-Lessard, P., Schinke, R., Bittererová, M., & Farantos, S. C. 2002, J. Chem. Phys., 116, 9749
Smith, M. A. H., Rinsland, C. P., Fridovich, B., & Rao, K. N. 1985, Mole. Spectrosc. Mod. Res., 3, 111
Soifer, B. T., Puetter, R. C., Russell, R. W., Willner, S. P., Harvey, P. M., & Gillett, F. C. 1979, ApJ, 232, L53
Spinks, J. W. T., & Woods, R. J. 1990, in An Introduction to Radiation Chemistry (3rd edn.; New York: Wiley)
Steinfeld, J. I., Francisco, J. S., & Hase, W. L. 1999, Chemical Kinetics and Dynamics (2nd edn.; Upper Saddle River, NJ: Prentice Hall)
Strazzulla, G., & Johnson, R. E. 1991, in Comets in the Post Halley Era, ed. R. L. Jr Newburn, M. Nuegebauer, & J. Rahe (Dordrecht: Kluwer), 243
Swallow, A. J. 1973, Radiation Chemistry (London: Longman)
Talbi, D., Chandler, G. S., & Rohl, A. L. 2006, Chem. Phys., 320, 214
Talbi, D., & Herbst, E. 2002, A&A, 386, 1139
Tielens, A. G. G. M., & Hagen, W. 1982, A&A, 114, 245
Tielens, A. G. G. M., Tokunaga, A. T., Geballe, T. R., & Baas, F. 1991, ApJ, 281, 181
Toth, R. A., Miller, C. E., Brown, L. R., Devi, V. M., & Benner, D. C. 2007, J. Mol. Spectrosc., 243, 43
Toth, R. A., Miller, C. E., Brown, L. R., Devi, V. M., & Benner, D. C. 2008, J. Mol. Spectrosc., 251, 64
Trottier, A., & Brooks, R. L. 2004, ApJ, 612, 1214
Watanabe, N., & Kouchi, A. 2002, ApJ, 567, 651
Whittet, D. C. B., Shenoy, S. S., Bergin, E. A., Chiar, J. E., Gerakines, P. A., Gibb, E. L., Melnick, G. J., & Neufeld, D. A. 2007, ApJ, 655, 332
Whittet, D. C. B., Cook, A. M., Chiar, J. E., Pendleton, Y. J., Shenoy, S. S., & Gerakines, P. A. 2009, ApJ, in press (arXiv:0901.0554v1[astro-ph.SR])
Wilson, R. W., Jefferts, K. B., & Penzias, A. A. 1970, ApJ, 161, L43
Woon, D. A. 2002, ApJ, 569, 541
Xantheas, S. S., & Ruedenberg, K. 1994, Int. J. Quantum Chem., 49, 409
Zetner, P. W., Kanik, I., & Trajmar, S. 1998, J. Phys. B: Opt. Mol. Phys., 31, 2395
Ziegler, J. F., Biersack, J. P., & Littmark, V. 1985, The Stopping and Range of Ions in Solids (New York: Permagon)